

How unconventional oxidation state Au^{2+} is stabilized in halide perovskite $\text{Cs}_4\text{Au}_3\text{Cl}_{12}$: a first-principles study of its polaron crystal nature

Kazuki Morita* and Andrew M. Rappe*

Department of Chemistry, University of Pennsylvania, Philadelphia, Pennsylvania 19104-6323, USA

E-mail: morita0@sas.upenn.edu; rappe@sas.upenn.edu

Abstract

Gold in crystalline compounds is typically only stable in oxidation states Au^{1+} and Au^{3+} . Even compounds with nominal Au^{2+} usually disproportionate into Au^{1+} and Au^{3+} . Recently, $\text{Cs}_4\text{Au}_3\text{Cl}_{12}$ was synthesized, where gold took the 2+ state in the bulk. Here, we investigate this compound using first-principles calculations and show that stabilization of the Au^{2+} ion is through the formation of a polaron crystal. The electronic and phononic structure suggest that the bonding network can be interpreted as a collection of $[\text{Au}^{2+}\text{Cl}_4]^{2-}$ and $[\text{Au}^{3+}\text{Cl}_4]^{1-}$ square planar motifs, and the crystal lacks a smooth pathway for Au^{2+} to disproportionate into Au^{1+} and Au^{3+} . The electronic states of Au are contained within each AuCl_4 motif, which allows for the Au^{2+} state to be localized and isolated electronically. The Au^{2+} -sites form an ordered structure, which is driven by a strong repulsive interaction between $[\text{Au}^{2+}\text{Cl}_4]^{2-}$ motifs due to their lattice distortion. The electron-phonon coupling between Au^{2+} and Cl explains

the stability of Au^{2+} , which suggests this material to be interpreted as a polaron crystal. By considering redox reaction, we show that $\text{Cs}_4\text{Au}_3\text{Cl}_{12}$ has the maximal density of Au^{2+} , and further oxidation will induce a delocalized state. $\text{Cs}_4\text{Au}_3\text{Cl}_{12}$ has distinctive electronic structure, with a narrow gap, isolated HOMO and LUMO bands strongly localized at the Au-sites, and magnetization at the Au^{2+} -sites making $\text{Cs}_4\text{Au}_3\text{Cl}_{12}$ unique among quantum materials. Magnetism in gold is rare, and $\text{Cs}_4\text{Au}_3\text{Cl}_{12}$ can be a testbed to explore novel gold chemistry as well as polaron crystal transport. The strategy to stabilize an unconventional oxidation state through engineering of lattice distortions is quite general; therefore, we propose that a similar approach will be applicable to a wide variety of transition metal compounds.

Introduction

As one of the foundational concepts in chemistry, oxidation state plays a central role in scientific research since the early days.¹ Indeed, ground-breaking materials development has often involved the realization of a particular oxidation state.^{2,3} Examples include enhancing the surface reactivity of catalysts,^{4–7} systematically tuning work functions,⁸ quantum criticality,⁹ and the emergence of superconductivity.^{10,11} Even so, each atomic species has a limited number of stable oxidation states, and realizing any unusual oxidation state is still a challenge.

Mixed-valence compounds are a particularly interesting class of materials, wherein a single constituent species takes multiple oxidation states.^{12–14} Unlike defects or dangling bonds at surfaces and interfaces, these species are homogeneously distributed across the material down to the unit cell level, and the disproportionated oxidation states are stable well beyond the time scale of phonon frequencies.¹² An intuitive and useful classification of mixed-valence compounds was proposed by Robin and Day, where class 1 is mixed-valence realized on different crystallographic sites, while class 3 has mixed valence on similar sites.¹³ Class 2 lies in between these two extremes and encompasses the majority of the known mixed-

valence materials.¹² One clear example of class 1 is in $P2_1/c$ Sn_3O_4 , where Sn^{2+} and Sn^{4+} occupy the peak of a triangular pyramid and the center of an octahedron, respectively.¹⁵ On the other hand, an example of class 2 close to 3 is the spin polaron crystal (Zener polaron) seen in $\text{Pr}_{0.6}\text{Ca}_{0.4}\text{MnO}_3$, where lattice distortion and charge couple strongly to form a periodic structure beyond the periodicity of the original lattice.¹⁶ Here, the environmental difference between Mn^{3+} and Mn^{4+} is attributed to polaronic lattice distortions. Numerous other strategies exist to stabilize mixed-valence, such as doping,¹⁷ designing a specific metal-organic framework structure,¹⁸ or as exotic as using light to switch between different charge orderings.¹⁹ Since class 3 can involve a nominal non-integer oxidation state, the charges can be ordered or fully delocalized. At present, the aim for mixed-valence materials is to realize class 1 or 2 mixed-valence materials and avoid class 3. However, thermal fluctuations, lattice strain, redox reaction, and instability of the Fermi level can drive the system towards delocalized class 3.²⁰ Therefore, to exhibit mixed-valence properties, compounds must be tolerant against these perturbations.

A recent noteworthy advance in the field of mixed-valence compounds is the synthesis of vacancy-ordered perovskite $\text{Cs}_4\text{Au}_3\text{Cl}_{12}$ with Au^{2+} and Au^{3+} .²¹ Not only is this material mixed-valence, but it is a rare case of Au^{2+} in a solid-state system, where only a handful of other examples are reported.^{22,23} The nominal electronic structure of $5d^9$ in Au^{2+} creates an unpaired spin and makes $\text{Cs}_4\text{Au}_3\text{Cl}_{12}$ a rare case where magnetism originates from gold. The conventional perovskite CsAuCl_3 , on the other hand, is also mixed-valence, but has Au^{1+} and Au^{3+} states.^{24,25} Since the oxidation state of transition metal species is strongly entangled with lattice distortion, one might expect strain and pressure to induce Au^{2+} , but both theory and experiment have shown that CsAuCl_3 turns metallic before Au^{2+} emerges.^{26,27} Therefore, the preference of gold to take 1+ and 3+ oxidation states is strong, and a strong mechanistic reason must be present in $\text{Cs}_4\text{Au}_3\text{Cl}_{12}$ in order to stabilize the Au^{2+} and prevent it from disproportionating.

In this work, we have investigated $\text{Cs}_4\text{Au}_3\text{Cl}_{12}$ using first-principles calculations and show

the validity of Au^{2+} and mechanism that stabilizes it. The structure of $\text{Cs}_4\text{Au}_3\text{Cl}_{12}$ has gold-vacancy ordering that allows every gold to bond with four chlorine atoms and form a square-planar AuCl_4 motif. This network has no excess Cl and lacks a smooth pathway to form Au^{1+} , providing a barrier against Au^{2+} disproportionating into Au^{1+} and Au^{3+} . The Au^{2+} is identifiably different from Au^{1+} and Au^{3+} due to its unpaired spin. The electronic and phononic band structures suggest that the Au^{2+} states are largely confined within the $[\text{Au}^{2+}\text{Cl}_4]^{2-}$ motif. This independence allows Au^{2+} to be stable as a form of isolated small polaron state, where interaction with the other Au^{2+} ions is minimal. At the same time, however, the $[\text{Au}^{2+}\text{Cl}_4]^{2-}$ motif, as a whole has a repulsive strain-field interaction to the other $[\text{Au}^{2+}\text{Cl}_4]^{2-}$, resulting in the Au^{2+} ions exhibiting an ordered structure. Unlike many mixed-valence compounds, we also show that $\text{Cs}_4\text{Au}_3\text{Cl}_{12}$ is stable against thermal fluctuations and redox reactions. Our results establish the validity and stability of Au^{2+} in $\text{Cs}_4\text{Au}_3\text{Cl}_{12}$ and that the stabilization mechanism is explained by the formation of a polaron crystal.

Results and Discussion

Structure and bonding

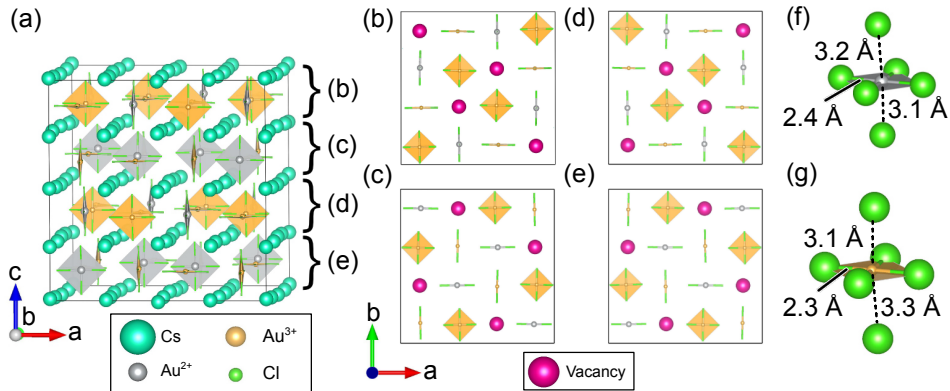


Figure 1: (a) Conventional unit cell of $\text{Cs}_4\text{Au}_3\text{Cl}_{12}$. (b)~(e) Cross section along successive (001) planes. (f) Distances to six nearest Cl around (f) Au^{2+} and (g) Au^{3+} .

The density functional theory (DFT) optimized structure of $\text{Cs}_4\text{Au}_3\text{Cl}_{12}$ is shown in

Figure 1(a), where it takes the tetragonal $I4_1cd$ (#110) space group. The structure can be understood as a vacancy-ordered perovskite, where one out of every four Au atoms is missing from CsAuCl_3 , forming $4 \times 4 \times 4$ superlattice. The Au-site is mixed-valence, taking oxidation states of Au^{2+} and Au^{3+} , which are presented in grey and yellow in Figure 1, respectively. Both Au-sites have six neighboring Cl-sites, but two of the Cl-sites are far ($\sim 35\%$ farther) and beyond the Cs-plane, therefore making it effectively a square-planar AuCl_4 bonding environment (Figures 1(f) and (g)). We, therefore, depict Au-sites as square AuCl_4 motifs showing the bonding to the four closest Cl-sites for the rest of the work. The cross-sectional views of the conventional cell along (001) planes are shown in Figure 1(b)-(e). One can find that any linear 4×1 set of Au-sites taken along any of the axes has two Au^{3+} -sites, a Au^{2+} -site, and a vacancy. None of the square-planar $[\text{Au}^{2+}\text{Cl}_4]^{2-}$ motifs lie in the (001); they lie in the (100) plane (Figure 1(b) and (d)) or the (010) plane (Figure 1(c) and (e)). Furthermore, any $[\text{AuCl}_4]$ has two vacancy cells next to it along two of its in-plane directions.

At first glance, the crystal structure seems complicated, as though a simpler crystal structure could exist. However, we show that the structure is uniquely determined by two conditions. Firstly, if we ignore the difference between the Au^{2+} and the Au^{3+} and only consider the connectivity of Au and Cl-ions, the structure is uniquely determined by assuring that each AuCl_4 has two Au-vacancies next to it (step-by-step explanation presented in Supplementary Information). Secondly, the Au^{2+} -site locations are determined by making sure that they do not neighbor each other. There are three unique ways to choose this, and each of the choices corresponds to selecting one axis as the c -axis for the tetragonal $I4_1cd$ structure. The tendency for Au^{2+} to repel each other was confirmed by calculating an artificial structure with two neighboring Au^{2+} -sites and finding it to be unstable. These two rules uniquely determine the $\text{Cs}_4\text{Au}_3\text{Cl}_{12}$ structure.

Here, the Au-vacancy plays a dual role of making enough Cl-sites available for gold to form the AuCl_4 motif and absorbing the strain caused by the larger size of Au^{2+} . In particular the two Au-vacancies next to each $[\text{Au}^{2+}\text{Cl}_4]^{2-}$ motif allow the Au^{2+} -Cl bonds to relax along the

in-plane directions and prevent the strain from propagating to the neighboring AuCl_4 motifs. Every Cl ion belongs to a AuCl_4 motif, so a smooth pathway to form Au^{1+} , where it takes linear bonding environment,²⁷ is not possible without forming an energetically unfavorable isolated Cl. The above geometrical argument explains the structural stability of $\text{Cs}_4\text{Au}_3\text{Cl}_{12}$, but it is based on a rudimentary ball-and-stick model. The validity of this simplified picture will be justified in the following sections.

Electronic structure

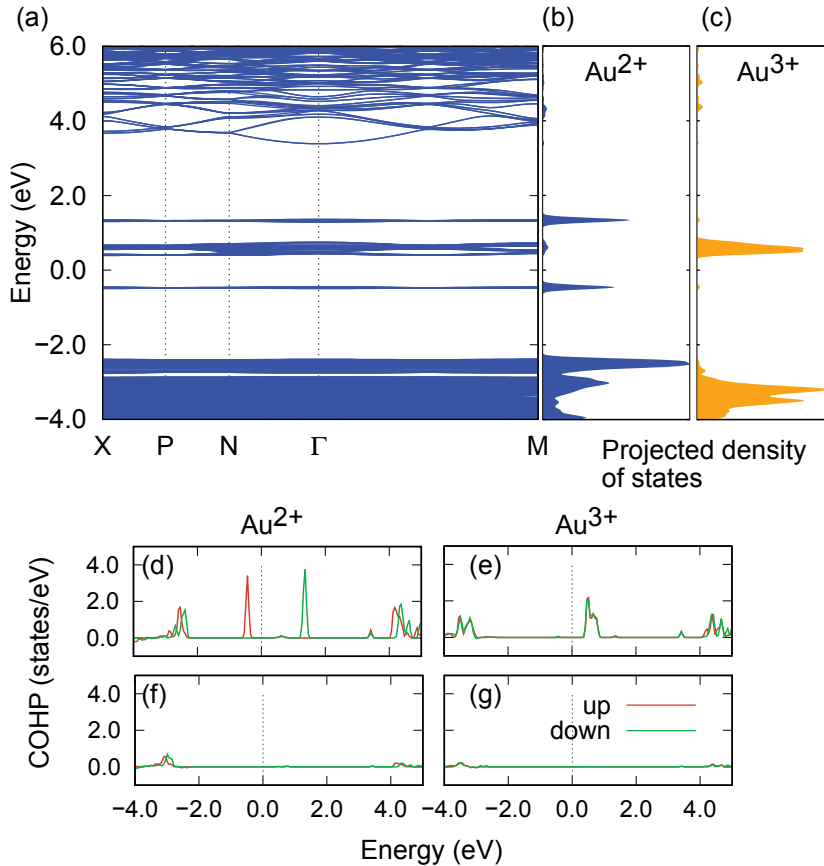


Figure 2: (a) Electronic band dispersion. Zero of energy is taken to be the center of the band gap. Projected density of states for (b) Au^{2+} and (c) Au^{3+} . Spin-resolved crystal orbital Hamilton population (COHP) of (d) nearest-neighbor Au^{2+} -Cl, (e) nearest-neighbor Au^{3+} -Cl, (f) second nearest-neighbor Au^{2+} -Cl, and (g) second nearest-neighbor Au^{3+} -Cl. Spin up and down are plotted with red and green, respectively.

$\text{Cs}_4\text{Au}_3\text{Cl}_{12}$ exhibits a distinctive electronic structure, where the valence and the conduction

tion band edges are isolated from the rest of the bands (Figure 2(a)). The isolated valence band edge is mainly composed of the Au^{2+} (Figure 2(b)), and the lowest conduction band is mainly composed of the Au^{3+} (Figure 2(c)). These states exhibits a small dispersion, suggesting that the gold states are highly localized. The band splitting in Au^{2+} is the result of the $d_{x^2-y^2}$ orbital becoming half-occupied. To elucidate the contribution of these states towards bonding, the parity of the wavefunction was analyzed using spin-resolved crystal orbital Hamilton population (COHP), which takes a positive value when the interaction between atoms is bonding.²⁸ Both Au^{2+} and Au^{3+} were only bonded to the nearest Cl-sites, and little interaction was present between Au and the second-nearest-neighbor Cl-sites. (Figure 2(d)-(g)). This supports the geometrical model that the crystal structure of $\text{Cs}_4\text{Au}_3\text{Cl}_{12}$ can be discussed based on the AuCl_4 motif.

We next assessed the validity of the Au^{2+} state by analyzing the charge around the Au^{2+} -site. The charge assignment was done via the wavefunction topology and the modern theory of polarization method.²⁹ We created a series of structures where four Au^{2+} ions are gradually displaced to the next Au^{2+} -site along the z-direction, equivalent to one Au^{2+} being displaced along the full length of the calculation cell in the z-direction (detailed path in supporting information). The current caused by this modification was evaluated using the Berry phase calculation, and the charge carried by Au^{2+} was indeed 2+. We also found that local positive charge was 30% larger around Au^{3+} than that around Au^{2+} using Bader charge analysis. Interestingly, the Born effective charges are very anisotropic, and the out-of-plane component was small (Table S3). More explicitly, Au^{2+} exhibits a finite magnetic moment of 0.43 μ_B (Au^{1+} and Au^{3+} show $\mu_B = 0$). This is a qualitative and quantitative difference only found for Au^{2+} . This magnetic moment interacted only weakly with other Au^{2+} ions, but it did showed a weak tendency to prefer an anti-ferromagnetic configuration (Table S4).

$\text{Cs}_4\text{Au}_3\text{Cl}_{12}$ belongs to a polar $I4_1cd$ space group and has a finite spontaneous polarization of 0.056 C/m². Interestingly, the spontaneous polarization is solely attributed to the difference between Au^{2+} and Au^{3+} -sites, therefore almost purely electronic in nature. The

spontaneous polarization can be reversed by Au^{2+} and Au^{3+} -site exchanging their locations. These properties also augment the quantitative difference between Au^{2+} and Au^{3+} . From the above results, we believe it is legitimate to consider Au^{2+} as 2+ oxidation state. The local environments around the Au^{2+} -site and the Au^{3+} -site are similar, and thus, in the language of Robin and Day, $\text{Cs}_4\text{Au}_3\text{Cl}_{12}$ is class 2, close to class 3.

Phononic structure

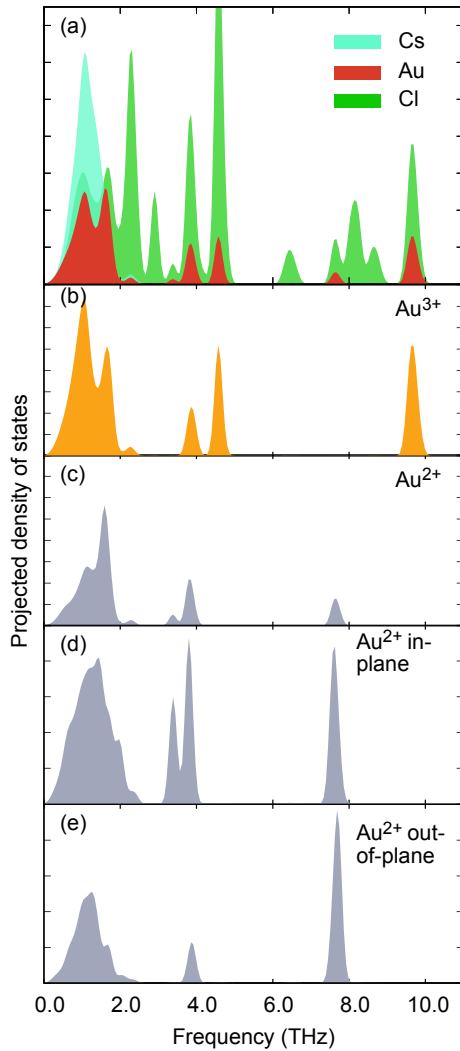


Figure 3: (a) Phonon-projected density of states for Cs, Au, and Cl. Phonon-projected density of states for (b) Au^{2+} and (c) Au^{3+} . Phonon-projected density of states for (d) in-plane and (e) out-of-plane $\text{Au}^{2+}-\text{Cl}$ direction.

Next, we look at the dynamical properties through the phonons. The projected phonon density of states (Figure 3(a)) suggests that the Cs vibration is localized around 1.0 THz, and the bands above 2.0 THz are mostly attributed to the Au and Cl atoms. This suggests that Cs is dynamically isolated from the rest of the lattice, as seen in perovskites.³⁰ Au-Cl interactions are largely encoded in the three groups of peaks above 2.0 THz, which had simultaneous contributions from Au and Cl: three peaks around 4.0 THz, a peak around 8.0 THz, and a peak around 10.0 THz. Within the Au spectra, Au^{2+} had consistently lower frequencies compared to Au^{3+} (Figures 3(b) and (c)). This is explained by the suppressed interaction between the Au^{2+} and Cl, due to the longer inter-atomic distance caused by the polaronic distortion. Further decomposition of the spectrum into in-plane direction (Figure 3(d)) and out-of-plane direction (Figure 3(e)) revealed that the lowest frequency peak around 4.0 THz was solely attributed to Au^{2+} vibrating in the in-plane directions. This suggests significantly stronger interaction within the $\text{Au}^{2+}\text{Cl}_4$ motif compared to the interaction with the neighbouring AuCl_4 motif. We also did not find any imaginary modes, suggesting $\text{Cs}_4\text{Au}_3\text{Cl}_{12}$ to be stable against thermal perturbations (Figure S10(a)).

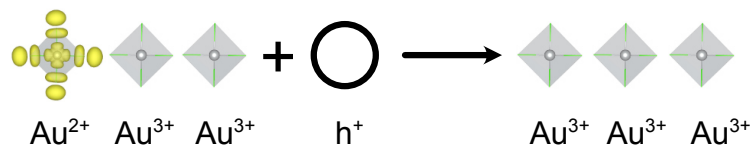
Redox stability

Since many mixed-valence compounds are unstable against redox reactions, we have analysed the redox stability of $\text{Cs}_4\text{Au}_3\text{Cl}_{12}$ by calculating the energy of the charged systems. First, we consider a situation where $\text{Cs}_4\text{Au}_3\text{Cl}_{12}$ is oxidised (Figure 4(a)). We found that the introduced extra hole localized at the Au^{2+} -site, forming Au^{3+} :

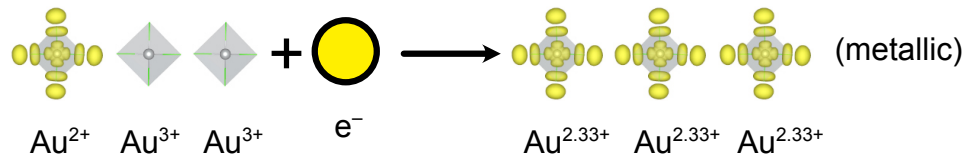


The reaction was an exothermic process with 0.40 eV energy difference per Au^{2+} , suggesting it occurs spontaneously. This reaction also indicates the energy released by freeing the lattice distortion caused by an Au^{2+} polaron, which corresponds to the polaron formation energy.

(a)



(b)



(c)

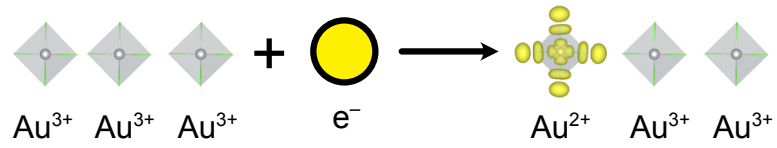
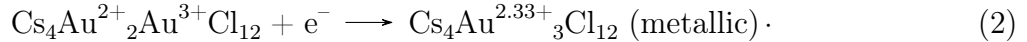


Figure 4: Schematic image of calculated chemical reactions. (a) oxidation, (b) reduction, and (c) reverse reaction of (a).

Next, we consider a reduction of $\text{Cs}_4\text{Au}_3\text{Cl}_{12}$ (Figure 4(b)). Instead of forming an extra Au^{2+} , the extra electron delocalized and formed a metallic $\text{Cs}_4\text{Au}_3\text{Cl}_{12}$,³¹



This suggests that the Au^{2+} density in $\text{Cs}_4\text{Au}_3\text{Cl}_{12}$ is saturated and that additional attempts to add an electron will cause the occupation of the conduction band. Finally, we also consider the inverse reaction of Equation 1 and consider reduction of $\text{Cs}_4\text{Au}^{3+}{}_3\text{Cl}_{12}$ (Figure 4(c)). Note that this differs from Equation 2 because the reaction starts with the oxidized state. In contrary to Equation 2, the extra electron localized at Au^{3+} -site forming Au^{2+} :



This further supports that Au^{2+} density in $\text{Cs}_4\text{Au}_3\text{Cl}_{12}$ is saturated.

The above results highlight the largely asymmetric nature of the Au^{2+} state stability against redox reactions. Equation 1 indicates that the removal of electrons can be done locally, which suggests that $\text{Cs}_4\text{Au}_3\text{Cl}_{12}$ is stable against modest oxidation. On the other hand, Equation 2 indicates instability against reduction. However, Equation 3 suggests that if the crystal is already oxidized, the effect of reduction can be local. Therefore, we suggest that experimentally synthesized $\text{Cs}_4\text{Au}_3\text{Cl}_{12}$ is oxidized from the stoichiometric $\text{Cs}_4\text{Au}_3\text{Cl}_{12}$ and that the synthesized samples must be moderately oxidized to retain the mixed-valence state.

The above results suggest that each $[\text{Au}^{2+}\text{Cl}]^{2-}$ motif behaves like an isolated polaron, and $\text{Cs}_4\text{Au}_3\text{Cl}_{12}$ is a ordered collection of them. The fact that the Au^{2+} cannot exist without Au-vacancy suggests it to be more similar to a polaron trapped near a defect rather than a self-trapped polaron. A similar concept of polaron crystal or polaron ordering has been reported in several manganese oxides.^{16,32-34} The distinctive behavior of a polaron crystal was suggested to be its temperature dependence, where the polaron crystalline order can

melt to change the observed transport properties drastically.^{32,33} In $\text{Cs}_4\text{Au}_3\text{Cl}_{12}$, however, such a polaron melting was not observed experimentally,²¹ suggesting the Au^{2+} to be more stable than other polaron crystals. The Au^{2+} states in $\text{Cs}_4\text{Au}_3\text{Cl}_{12}$ were largely independent electronically and magnetically; however, the strain field created by each $[\text{Au}^{2+}\text{Cl}_4]^{2-}$ motif interacted strongly and resulted in the ordered Au^{2+} structure. This is in contrast to the case of manganese oxides, where strong electronic and magnetic interactions dominate the polaronic behavior.^{16,34} Therefore, the approach of using lattice distortion to control oxidation state is widely applicable, but depending on the system, the resulting properties will likely differ substantially.

Conclusion

We have shown that lattice distortion can be a useful lever to control oxidation state. Structurally $\text{Cs}_4\text{Au}_3\text{Cl}_{12}$ is a collection of independent Cs^+ , $[\text{Au}^{2+}\text{Cl}_4]^{2-}$, and $[\text{Au}^{3+}\text{Cl}_4]^{1-}$ sites, where bonds between these entities are weak. The structure lacks a smooth pathway toward Au^{1+} formation, which prevents the Au^{2+} from disproportionating. We provided evidence that Au^{2+} is indeed a 2+ through charge analyses and observation of a finite magnetic moment. The localized Au^{2+} state was stabilized through strong trapping of a hole at each adjacent Au^{3+} site, suggesting this crystal to be interpreted as a polaron crystal. The Au^{2+} state is likely to be stable against thermal and electronic perturbation. Each Au^{2+} is electronically and magnetically independent, but at the same time, the strain-field interaction is strong, leading to repulsion between Au^{2+} ions. Our calculations also suggested that $\text{Cs}_4\text{Au}_3\text{Cl}_{12}$ has a saturated Au^{2+} density, and reduction is predicted to cause it to become metallic. Furthermore, the rare Au magnetism in $\text{Cs}_4\text{Au}_3\text{Cl}_{12}$ will open an avenue for gold magnetism chemistry, which is still largely unexplored. Coupling with lattice distortion is common across transition-metal elements and suggests that an analogous approach could lead to polaron crystal design for accessing unconventional oxidation states and novel chem-

istry in many other transition-metal compounds.

Methodology

Pseudopotential plane-wave DFT calculations were performed using the VASP code.^{35,36} For reciprocal lattice sampling, a Monkhorst-Pack sampling was adopted, with spacing at most 0.28 \AA^{-1} between the neighboring k-points and a plane-wave cutoff of at least 400 eV. 9, 11, and 7 valence and/or semi-core electrons were considered for Cs, Au, and Cl, respectively. The hybrid exchange-correlation functional (HSE06) was used throughout the work,³⁷ except for the phonon calculation, where PBE+ U ($U=3.4$ eV) was used. The Hubbard U was applied to the Au 5d-orbital, and the rotational invariant approach suggested by Dudarev et al. was used.³⁸ Phonon modes were calculated in a 152-atom primitive cell using the phonopy package, and eigenvectors of the phonon bands were projected onto an atomic basis to analyze their contributions.^{39,40}

The initial structure for the DFT calculations was taken from a structure reported by Karunadasa and co-workers²¹ and was subsequently relaxed. Spontaneous polarization was calculated using the Berry phase method in the modern theory of polarization.⁴¹⁻⁴³ An inverse-polarization pair was generated by creating a mirror image structure where an electron at the Au^{2+} hops two site along $-z$ direction to a Au^{3+} -site. The narrow band gap of this material made the perturbative approach numerically unstable, so the Born effective charge was calculated by a finite displacement method. Symmetry analysis was done using Spglib and ISOTROPY software. The bader charge analysis was performed with analysis code developed by Henkelman and co-workers.⁴⁴ COHP was calculated by the LOBSTER package, where six Cl-sites around all Au-sites were considered.²⁸

The wavefunction topology and the modern theory of polarization method was used to analyze the nominal charge of Au^{2+} .²⁹ We displaced four Au^{2+} along the z-direction to the next Au^{2+} -site so that each Au^{2+} moves 25% of the calculation cell (more details in supporting

information). In other words, a current was generated equivalent to moving Au^{2+} by one full supercell lattice vector in the z-direction, restoring the original structure through periodic boundary conditions. The initial and the final structures were equivalent, so the change in the Berry phase is always an integer multiple of 2π , or n times the polarization quantum. This n plus the nuclear charge is the oxidation state of the ion.

Redox reaction was modeled by calculating charged systems, where +1 and -1 was considered for oxidized and reduced $\text{Cs}_4\text{Au}_3\text{Cl}_{12}$, respectively. As commonly done in periodic boundary conditions, we calculated charged systems with a neutralizing background charge. To remove spurious interactions between periodic image charges, we applied the Kumagai-Oba correction (extended Freysoldt-Neugebauer-Van de Walle correction).^{45,46} This correction was not applied to the -1 charged case, where the extra electron was delocalized and thus compensated the background charge without correction. The stability of different charge states as a function of the Fermi level was calculated referencing the neutral charge state as zero of energy and the valence band maximum as zero of the Fermi level.

Acknowledgement

The authors thank Churlhi Lyi and Youngkuk Kim for fruitful discussions. K.M. and A.M.R. acknowledge support from the U.S. Department of Energy, Office of Science, Office of Basic Energy Sciences, under Award #DE-SC0021118. Computational support was provided by the National Energy Research Scientific Computing Center (NERSC), a U.S. Department of Energy, Office of Science User Facility located at Lawrence Berkeley National Laboratory, operated under Contract No. DE-AC02-05CH11231. K.M. acknowledges the JSPS Overseas Research Fellowship.

Supplementary Information

The following additional results are presented in the Supplementary Information.

- Uniqueness of the $\text{Cs}_4\text{Au}_3\text{Cl}_{12}$ structure
- Primitive cell structure and coordinates
- Full Born effective charges
- Spontaneous polarization branch
- COHP for all the nearest neighbors
- Comparison of the magnetic orders
- Polarization change induced by the Au^{2+} current
- Effect of the Au^{2+} – Cl bond length on Au^{2+}
- Phonon dispersion
- Fermi energy dependence of Au^{2+} stability

References

- (1) Pauling, L. *The Nature of the Chemical Bond*, 3rd ed.; Cornell university press Ithaca, NY, 1960.
- (2) Kageyama, H.; Hayashi, K.; Maeda, K.; Attfield, J. P.; Hiroi, Z.; Rondinelli, J. M.; Poeppelmeier, K. R. Expanding frontiers in materials chemistry and physics with multiple anions. *Nature Communications* **2018**, *9*.
- (3) Walsh, A.; Sokol, A. A.; Buckeridge, J.; Scanlon, D. O.; Catlow, C. R. A. Oxidation states and ionicity. *Nature Materials* **2018**, *17*, 958–964.
- (4) Bai, Y.; Wu, Y.; Zhou, X.; Ye, Y.; Nie, K.; Wang, J.; Xie, M.; Zhang, Z.; Liu, Z.; Cheng, T.; Gao, C. Promoting nickel oxidation state transitions in single-layer NiFeB hydroxide nanosheets for efficient oxygen evolution. *Nature Communications* **2022**, *13*.

- (5) De Luna, P.; Quintero-Bermudez, R.; Dinh, C.-T.; Ross, M. B.; Bushuyev, O. S.; Todorović, P.; Regier, T.; Kelley, S. O.; Yang, P.; Sargent, E. H. Catalyst electro-redistribution controls morphology and oxidation state for selective carbon dioxide reduction. *Nature Catalysis* **2018**, *1*, 103–110.
- (6) Jiang, Y.; Shan, J.; Wang, P.; Huang, L.; Zheng, Y.; Qiao, S.-Z. Stabilizing Oxidation State of SnO₂ for Highly Selective CO₂ Electroreduction to Formate at Large Current Densities. *ACS Catalysis* **2023**, *13*, 3101–3108.
- (7) Yang, P.-P. et al. Protecting Copper Oxidation State via Intermediate Confinement for Selective CO₂ Electroreduction to C²⁺ Fuels. *Journal of the American Chemical Society* **2020**, *142*, 6400–6408.
- (8) Greiner, M. T.; Chai, L.; Helander, M. G.; Tang, W.; Lu, Z. Transition Metal Oxide Work Functions: The Influence of Cation Oxidation State and Oxygen Vacancies. *Advanced Functional Materials* **2012**, *22*, 4557–4568.
- (9) Matsumoto, Y.; Nakatsuji, S.; Kuga, K.; Karaki, Y.; Horie, N.; Shimura, Y.; Sakakibara, T.; Nevidomskyy, A. H.; Coleman, P. Quantum Criticality Without Tuning in the Mixed Valence Compound β -YbAlB₄. *Science* **2011**, *331*, 316–319.
- (10) Wang, Y.; Sato, H.; Toda, Y.; Ueda, S.; Hiramatsu, H.; Hosono, H. SnAs with the NaCl-type Structure: Type-I Superconductivity and Single Valence State of Sn. *Chemistry of Materials* **2014**, *26*, 7209–7213.
- (11) Note that oxidation states can be ill-defined for metals.
- (12) Varma, C. M. Mixed-valence compounds. *Reviews of Modern Physics* **1976**, *48*, 219–238.
- (13) Day, P.; Hush, N. S.; Clark, R. J. Mixed valence: origins and developments. *Philosophical Magazine* **1972**, *17*, 103–124.

sophical Transactions of the Royal Society A: Mathematical, Physical and Engineering Sciences **2007**, *366*, 5–14.

- (14) Krick, A. L.; Lee, C.; Sichel-Tissot, R. J.; Rappe, A. M.; May, S. J. Interplay between Cation and Charge Ordering in $\text{La}_{1/3}\text{Sr}_{2/3}\text{FeO}_3$ Superlattices. *Advanced Electronic Materials* **2016**, *2*.
- (15) Manikandan, M.; Tanabe, T.; Li, P.; Ueda, S.; Ramesh, G. V.; Kodiyath, R.; Wang, J.; Hara, T.; Dakshanamoorthy, A.; Ishihara, S.; Ariga, K.; Ye, J.; Umezawa, N.; Abe, H. Photocatalytic Water Splitting under Visible Light by Mixed-Valence Sn_3O_4 . *ACS Applied Materials & Interfaces* **2014**, *6*, 3790–3793.
- (16) Daoud-Aladine, A.; Rodríguez-Carvajal, J.; Pinsard-Gaudart, L.; Fernández-Díaz, M. T.; Revcolevschi, A. Zener Polaron Ordering in Half-Doped Manganites. *Physical Review Letters* **2002**, *89*.
- (17) Zhou, F.; Maxisch, T.; Ceder, G. Configurational Electronic Entropy and the Phase Diagram of Mixed-Valence Oxides: The Case of Li_xFePO_4 . *Physical Review Letters* **2006**, *97*.
- (18) Park, J. G.; Aubrey, M. L.; Oktawiec, J.; Chakarawet, K.; Darago, L. E.; Grandjean, F.; Long, G. J.; Long, J. R. Charge Delocalization and Bulk Electronic Conductivity in the Mixed-Valence Metal–Organic Framework $\text{Fe}(1,2,3\text{-triazolate})_2(\text{BF}_4)_x$. *Journal of the American Chemical Society* **2018**, *140*, 8526–8534.
- (19) Matsumoto, T.; Newton, G. N.; Shiga, T.; Hayami, S.; Matsui, Y.; Okamoto, H.; Kumai, R.; Murakami, Y.; Oshio, H. Programmable spin-state switching in a mixed-valence spin-crossover iron grid. *Nature Communications* **2014**, *5*.
- (20) Brunschwig, B. S.; Creutz, C.; Sutin, N. Optical transitions of symmetrical mixed-valence systems in the Class II–III transition regime. *Chemical Society Reviews* **2002**, *31*, 168–184.

- (21) Lindquist, K. P.; Eghdami, A.; Deschene, C. R.; Heyer, A. J.; Wen, J.; Smith, A. G.; Solomon, E. I.; Lee, Y. S.; Neaton, J. B.; Ryan, D. H.; Karunadasa, H. I. Stabilizing Au^{2+} in a mixed-valence 3D halide perovskite. *Nature Chemistry* **2023**,
- (22) Elder, S. H.; Lucier, G. M.; Hollander, F. J.; Bartlett, N. Synthesis of Au(II) Fluoro Complexes and Their Structural and Magnetic Properties. *Journal of the American Chemical Society* **1997**, *119*, 1020–1026.
- (23) Hwang, I.-C.; Seppelt, K. The Reduction of AuF_3 in Super Acidic Solution. *Zeitschrift für anorganische und allgemeine Chemie* **2002**, *628*, 765.
- (24) Ushakov, A. V.; Streletsov, S. V.; Khomskii, D. I. Crystal field splitting in correlated systems with negative charge-transfer gap. *Journal of Physics: Condensed Matter* **2011**, *23*, 445601.
- (25) Debbichi, L.; Lee, S.; Cho, H.; Rappe, A. M.; Hong, K.; Jang, M. S.; Kim, H. Mixed Valence Perovskite $\text{Cs}_2\text{Au}_2\text{I}_6$: A Potential Material for Thin-Film Pb-Free Photovoltaic Cells with Ultrahigh Efficiency. *Advanced Materials* **2018**, *30*, 1707001.
- (26) Winkler, B.; Pickard, C. J.; Segall, M. D.; Milman, V. Density-functional study of charge disordering in $\text{Cs}_2\text{Au}(\text{I})\text{Au}(\text{III})\text{Cl}_6$ under pressure. *Physical Review B* **2001**, *63*.
- (27) Morita, K.; Rappe, A. M. Inverted Band Gap Trend through Octahedral Ordering in $\text{Cs}_2\text{Au}_2\text{X}_6$ ($\text{X} = \text{Cl}$, Br , and I). *Chemistry of Materials* **2024**, *36*, 5805–5813.
- (28) Maintz, S.; Deringer, V. L.; Tchougréeff, A. L.; Dronskowski, R. LOBSTER: A tool to extract chemical bonding from plane-wave based DFT. *Journal of Computational Chemistry* **2016**, *37*, 1030–1035.
- (29) Jiang, L.; Levchenko, S. V.; Rappe, A. M. Rigorous definition of oxidation states of ions in solids. *Physical review letters* **2012**, *108*, 166403.

- (30) Morita, K.; Davies, D. W.; Butler, K. T.; Walsh, A. Breaking the Aristotype: Feature-
ization of Polyhedral Distortions in Perovskite Crystals. *Chemistry of Materials* **2022**,
34, 562–573.
- (31) Note that the oxidation state of $\text{Au}^{2.33+}$ is a nominal value.
- (32) Mannella, N.; Yang, W. L.; Tanaka, K.; Zhou, X. J.; Zheng, H.; Mitchell, J. F.; Za-
anan, J.; Devereaux, T. P.; Nagaosa, N.; Hussain, Z.; Shen, Z.-X. Polaron coherence
condensation as the mechanism for colossal magnetoresistance in layered manganites.
Physical Review B **2007**, *76*.
- (33) Jooss, C.; Wu, L.; Beetz, T.; Klie, R. F.; Beleggia, M.; Schofield, M. A.; Schramm, S.;
Hoffmann, J.; Zhu, Y. Polaron melting and ordering as key mechanisms for colossal
resistance effects in manganites. *Proceedings of the National Academy of Sciences* **2007**,
104, 13597–13602.
- (34) Yamada, Y.; Hino, O.; Nohdo, S.; Kanao, R.; Inami, T.; Katano, S. Polaron Ordering
in Low-Doping $\text{La}_{1-x}\text{Sr}_x\text{MnO}_3$. *Physical Review Letters* **1996**, *77*, 904–907.
- (35) Kresse, G.; Furthmüller, J. Efficient iterative schemes for ab initio total-energy calcu-
lations using a plane-wave basis set. *Physical Review B* **1996**, *54*, 11169.
- (36) Kresse, G.; Joubert, D. From ultrasoft pseudopotentials to the projector augmented-
wave method. *Physical Review B* **1999**, *59*, 1758.
- (37) Heyd, J.; Scuseria, G. E.; Ernzerhof, M. Hybrid functionals based on a screened
Coulomb potential. *The Journal of Chemical Physics* **2003**, *118*, 8207–8215.
- (38) Dudarev, S. L.; Botton, G. A.; Savrasov, S. Y.; Humphreys, C. J.; Sutton, A. Electron-
energy-loss spectra and the structural stability of nickel oxide: An LSDA+ U study.
Physical Review B **1998**, *57*, 1505.

- (39) Togo, A.; Chaput, L.; Tadano, T.; Tanaka, I. Implementation strategies in phonopy and phono3py. *Journal of Physics: Condensed Matter* **2023**, *35*, 353001.
- (40) Togo, A. First-principles Phonon Calculations with Phonopy and Phono3py. *Journal of the Physical Society of Japan* **2023**, *92*.
- (41) Zak, J. Berry's phase for energy bands in solids. *Physical Review Letters* **1989**, *62*, 2747–2750.
- (42) Resta, R. Theory of the electric polarization in crystals. *Ferroelectrics* **1992**, *136*, 51–55.
- (43) King-Smith, R. D.; Vanderbilt, D. First-principles investigation of ferroelectricity in perovskite compounds. *Physical Review B* **1994**, *49*, 5828.
- (44) Henkelman, G.; Arnaldsson, A.; Jónsson, H. A fast and robust algorithm for Bader decomposition of charge density. *Computational Materials Science* **2006**, *36*, 354–360.
- (45) Freysoldt, C.; Neugebauer, J.; Van de Walle, C. G. Fully *Ab Initio* Finite-Size Corrections for Charged-Defect Supercell Calculations. *Physical Review Letters* **2009**, *102*, 016402.
- (46) Kumagai, Y.; Oba, F. Electrostatics-based finite-size corrections for first-principles point defect calculations. *Physical Review B* **2014**, *89*, 195205.